ADVANCED FUNCTIONAL MATERIALS

FULL PAPER

DOI: 10.1002/adfm.200800951

Catalyst-Free Efficient Growth, Orientation and Biosensing Properties of Multilayer Graphene Nanoflake Films with Sharp Edge Planes**

By *Nai Gui Shang, Pagona Papakonstantinou,* Martin McMullan, Ming Chu, Artemis Stamboulis, Alessandro Potenza, Sarnjeet S. Dhesi,* and *Helder Marchetto*

We report a novel microwave plasma enhanced chemical vapor deposition strategy for the efficient synthesis of multilayer graphene nanoflake films (MGNFs) on Si substrates. The constituent graphene nanoflakes have a highly graphitized knife-edge structure with a 2–3 nm thick sharp edge and show a preferred vertical orientation with respect to the Si substrate as established by near-edge X-ray absorption fine structure spectroscopy. The growth rate is approximately 1.6 μm min^{-1}, which is 10 times faster than the previously reported best value. The MGNFs are shown to demonstrate fast electron-transfer (ET) kinetics for the $Fe(CN)_6^{3-/4-}$ redox system and excellent electrocatalytic activity for simultaneously determining dopamine (DA), ascorbic acid (AA) and uric acid (UA). Their biosensing DA performance in the presence of common interfering agents AA and UA is superior to other bare solid-state electrodes and is comparable only to that of edge plane pyrolytic graphite. Our work here, establishes that the abundance of graphitic edge planes/defects are essentially responsible for the fast ET kinetics, active electrocatalytic and biosensing properties. This novel edge-plane-based electrochemical platform with the high surface area and electrocatalytic activity offers great promise for creating a revolutionary new class of nanostructured electrodes for biosensing, biofuel cells and energy-conversion applications.

1. Introduction

Although various carbon-based materials, such as highly ordered pyrolytic graphite (HOPG), glassy carbon, fullerenes, boron-doped diamond, carbon nanotubes (CNTs), etc.,[1] have been used as electrodes in both electroanalysis and electrocatalysis over the past decades, the individual roles of electrochemical activity of graphitic edges and metal impurities still remain open questions.[2,3] Highly anisotropic graphene materials such as HOPG and vertically oriented CNT arrays or forests can serve as excellent electrodes because they make predominant use of the highly reactive edge planes in contrast to the nearly inert basal planes. However, HOPG is very expensive and needs careful polishing to expose the fresh edge planes while most CNT arrays or forests always possess metal nanoparticles inherited by their metal catalytic chemical vapor deposition. It was found recently that the catalytically grown CNTs even after multiple purifications in strong acids for long times still contain residual metals sheathed by multilayer graphene layers, which not only lead to potential misinterpretations of electrochemical experiment but also can significantly affect their electrochemical repeatability and stability.[4,5]

Recently, graphene has been considered as a ''rising-star'' material and has received intensive attention because of its novel properties.[6] Here we report one kind of graphene integrated nanomaterial, that is, uniform multilayer graphene nanoflake films (MGNFs, also called carbon nanowalls, nanoflakes, nanosheets, and petals).[7–9] MGNFs could compete with HOPG and CNTs as they are made of vertical 1–20 nm thick, two-dimensional graphenes, which contain a large amount of open graphitic edge planes with high surface activity.[10] This is especially attractive as they were proved to be fabricated without the use of catalysts, although their growth mechanism is still not well understood. Thus, in contrast to aligned CNTs, the MGNFs could be one of best electrode materials to investigate basic electrochemical

[*] Dr. P. Papakonstantinou, Dr. N. G. Shang, and M. McMullan
Nanotechnology and Integrated Bio-Engineering Centre (NIBEC)
University of Ulster
Shore Road, Newtownabbey, BT37 0QB (UK)
E-mail: p.papakonstantinou@ulster.ac.uk
M. Chu, Dr. A. Stamboulis
Department of Metallurgy and Materials, University of Birmingham
Edgbaston, Birmingham, B15 2TT (UK)
Dr. A. Potenza, Dr. S. S. Dhesi, Dr. H. Marchetto
Diamond Light Source
Chilton, Oxfordshire, OX11 0DE (UK)

[**] We acknowledge supports from the European Union under the DESYGN-IT project (STREP Project 505626-1) and the National Centre for Electron Spectroscopy and Surface (NCESS) analysis at Daresbury Laboratory, UK. We thank R. McCann and A. Kumar in University of Ulster for their help in the X-ray photoelectron spectroscopy measurement. Supporting Information is available online from Wiley InterScience or from the author.

ADVANCED FUNCTIONAL MATERIALS

phenomena. Nevertheless, no information has been reported on the preferential orientation, electrochemical, and bioelectrocatalytic actions of MGNFs so far.

Dopamine (DA) is a neurotransmitter that plays a very important role in the central nervous, renal, hormonal, and cardiovascular systems.[11] Changes in the concentration of DA are closely linked to a human's health status. Thus, its detection has gained significant attention. Rapid, simple, and sensitive electrochemical methods have shown a huge potential in the neurotransmission detection. However, at traditional solid electrodes, DA and its coexisting species ascorbic acid (AA) and uric acid (UA) have an overlapping voltammetric response, resulting in rather poor selectivity and sensitivity. Thus, it is a challenge to distinguish the coexistence of DA, AA, and UA in a biological environment. Up to now, electrochemical pretreatment and various modified electrodes have been investigated to selectively determine DA in the presence of AA and UA.[12,13] For example, nafion[14] polypyrrole,[15] and stearic acid[16] membranes were used to selectively determine DA by means of their cationic permeability. Although the sensitivity and selectivity increase on modified electrodes, they suffer from some drawbacks. For example, they require time-consuming multiple modification steps. They are assembled in an ill-defined way and do not exhibit a reproducible area and a stable behavior. Therefore, it is of interest to explore novel electrode materials and analytic methods to sense DA conveniently, reproducibly with high sensitivity and selectivity.[17]

Meanwhile, direct growth of high-purity MGNFs on silicon wafers is especially attractive because the compatibility of the sensing element with conventional Si electronics could give the opportunity to fabricate completely integrated bioelectronic systems. However, the growth rate of uniform MGNFs currently deposited on flat substrates, is quite low (approximately 10 $\mu m\ h^{-1}$) except for bulk MGNF aggregates grown on the four sharp corners of a cubic metal holder, where the role of metal at the growth stage can not be neglected.[18,19]

In this paper, we report a simple and efficient method, called substrate-lift-up for the rapid growth of uniform MGNFs with sharp edges directly on the Si substrate without use of metal catalysts or any surface pre-treatments by means of microwave-assisted plasma chemical vapor deposition (MPCVD). The surface morphology, microstructure, orientation and chemical composition of as-deposited MGNFs were characterized by using scanning electron microscopy (SEM, FEI Quanta TA200 30), transmission electron microscopy (TEM), Raman spectroscopy (Labram 300), near-edge X-ray absorption fine structure (NEXAFS, at Diamond Synchrotron Light Source) spectroscopy, and high-resolution X-ray photoelectron spectroscopy (XPS, Scienta-ESCA300 spectrometer, at Daresbury Synchrotron Laboratory), respectively. Their electron-transfer (ET) properties were systematically investigated by cyclic voltammetry using the redox of $Fe(CN)_6^{3-/4-}$. The biosensing properties of MGNFs for the selective discrimination of DA in the presence of AA and UA were also explored for the first time and demonstrated the highly electrocatalytic activity of the edge planes.

2. Results and Discussion

2.1. Microstructure of MGNFs

It was found that MGNFs with same surface morphology can be deposited with a wide range (10–40%) of methane concentration (Fig. 1). Figure 1a and b show typical SEM images taken from samples deposited using 40% methane for 40 s and 30 min, respectively. It can be seen that the films consist of petal-like graphitic nanoflakes with very sharp edges, which randomly interlaced together and formed a nest-like porous structure with a large surface area (see Fig. 1c). Although the films deposited for 40 s and 30 min are essentially uniform, the constituent graphene nanoflakes are quite different in lateral size: 1–5 μm for 30-min deposition and 100–500 nm for 40-s deposition. Figure 1d is a cross sectional SEM image of MGNFs, showing that the majority of graphene nanoflakes have a preferentially vertical orientation with respect to the Si substrate, with a few of them been parallel to the substrate (see Fig. 1f). This kind of structural orientation allows the surface to be terminated with a large fraction of graphitic edge planes, which possess a higher surface activity compared to the basal graphitic plane. Thus, excellent electrochemical properties for MGNFs can be anticipated.

To conveniently observe the microstructure of MGNFs by TEM without any structural damage, MGNFs were directly deposited on a Mo grid under the same conditions and found to have the same morphology as those on Si. Then, the Mo grid with MGNFs was put on the top of another Cu grid for the

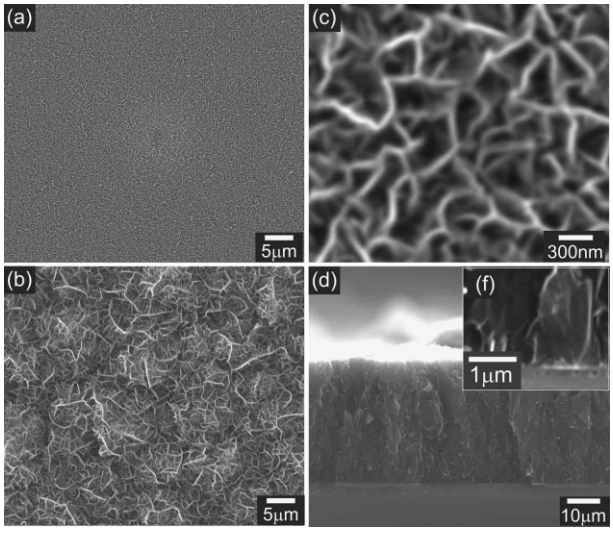

Figure 1. SEM images of MGNFs deposited for 40 s (a) and 30 min (b); c) is an enlarged image of (a); d) is a cross sectional SEM image of MGNFs deposited for 30 min; f) is an enlarged image of (d), showing the nanoflake preferentially vertical to the Si substrate.

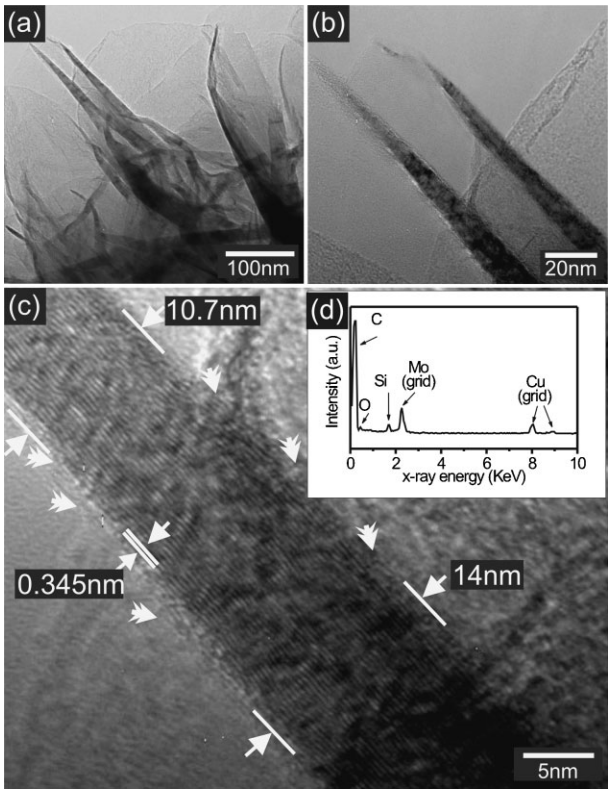

Figure 2. a) and b) Different magnification TEM images of MGNFs; c) High resolution TEM image of MGNFs, showing the nanoflake has a knife-edge or conical structure with open graphitic planes; d) EDS spectrum, showing the chemical composition of MGNF films.

TEM observation. Figure 2a and b are TEM images of MGNFs with different magnifications, deposited on the Mo grid. The nanoflakes are like narrow belts or bent leaves. Some of them show a knife-edge or a conical structure with a 20-nm-thick base and a 2–3-nm-thick sharp edge made of perfect graphitic layer with a (002) plane spacing of 0.345 nm (see Fig. 2c). On the edge of the sharp nanoflake there are many open graphitic layers and steps, which could serve not only as growth sites of MGNFs but also as potential adsorption sites of various atoms or species and emission sites of electrons.[10,20] The plane spacing measured from different nanoflakes is in the range between 0.345–0.36 nm, which is considerably closer to that of single-crystal graphite (0.335 nm) in comparison to carbon nanosheets previously reported.[9] In contrast to carbon nanowalls on SiO_2, no distinct amorphous layers were found on the outside of nanoflakes.[18] Energy dispersive X-ray microprobe spectroscopy (EDS) was used to analyze the chemical composition of the MGNF films in the TEM system. No traces of any other metals were found except for Mo and Cu, which both originate from the grids used (see Fig. 2d). The small amount of Si present stems from the Si support, diffused during the high-temperature deposition. Thus, the MGNFs deposited by our method have a higher crystalline quality than any other carbon nanowalls and nanosheets previously reported.

2.2. Orientation of MGNFs

NEXAFS is a non-destructive and powerful technique for studying the local electronic structure of thin films and adsorbates, etc. and recently has been widely used to assess the alignment of both carbon nanotubes and organic substances, by changing the angle (ϕ) between the electrical field vector (E) of incident polarized X-ray and the normal of sample surface, based on a polarized X-ray resonant absorption principle.[21,22] The measurements of NEXAFS were carried out at room temperature in Beam line I06 of the Diamond Synchrotron Radiation Light, UK. The C K-edge of MGNFs was collected in surface-sensitive total-electron-yield mode over the energy of 280–320 eV and normalized by dividing the flux curve recorded from a clean Au grid. Figure 3a shows the angle-dependent C K-edge NEXAFS spectra taken from the MGNFs. There are two prominent peaks located at 285.5 and 292.5 eV in all spectra, corresponding to the two specifically resonant transitions from the C 1s core level to two 2p unoccupied states, that is, $1s \rightarrow \pi^*$ and $1s \rightarrow \sigma^*$, respectively. A weak broad band centered at 288.9 eV, which originates from either $1s \rightarrow \pi^*$ (C–H) or $1s \rightarrow \pi^*$ (C=O) transitions because of the surface hydrogenated or oxygenated functionalities,[23] can be seen more clearly at the collecting angle of 30°. This suggests that hydrogen (C–H) and oxygen (C=O)

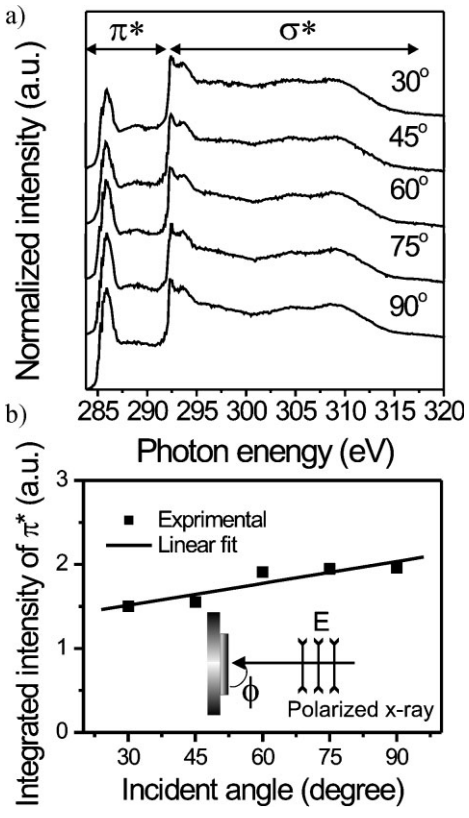

Figure 3. a) Angle dependent NEXAFS spectra of MGNFs; b) Integrated intensity of π^* peak versus the incident angle of polarized X-ray. The inset of (b) showing a geometric configuration between incident polarized X-ray and the surface normal of sample.

ADVANCED FUNCTIONAL MATERIALS

species could adsorb on the open graphitic layers found by TEM. As we know, the σ^* orbit is localized within the graphitic basal plane, while the π^* orbit is orthogonal to the σ^* orbit and thus parallel to the graphitic edge plane. The density of states of π^* and σ^* orbits can be presented by the resonant absorption transition of polarized X-ray in the NEXAFS spectra. Thus, we are able to infer the orientation of carbon-based materials from the angle dependence of C K-edge integrated intensity of NEXAFS spectra based on the geometric relation between graphitic basal (edge) planes and σ^* (π^*) orbits. Figure 3b shows the integrated intensity of π^* peak as a function of the incident angle of polarized X-ray. It is clear that the integrated intensity slightly increases with increasing the angle of incidence. To evaluate the degree of orientation in the MGNFs, we define an orientation parameter (OP) as[21,22]

$$OP = (I_\perp - I_\parallel)/(I_\perp + I_\parallel) \quad (1)$$

where $I_\perp$ and $I_\parallel$ are the π^* integrated intensities at normal incidence ($\phi = 90^\circ$) and grazing incidence ($\phi = 0^\circ$), respectively. The value of $I_\parallel$ at 0° can be obtained from a linear extrapolation of the fit curve to zero in Figure 3b. Note, a value close to 1 indicates that the basal graphitic plane has a higher degree of vertical orientation with respect to the substrate, while a value close to -1 is for a basal graphitic plane almost parallel to the substrate. Quantitative analysis shows that the OP for MGNFs is about 0.22, whose absolute value is less than those of HOPG (OP: -0.8 to -0.9) and aligned carbon nanotubes (OP: 0.4–0.5) but larger than those of single-walled CNT bucky paper (OP: -0.09) and powder (OP: 0.04). This unequivocally indicates the MGNFs have a preferentially vertical orientation with respect to the Si substrate, consistent with the SEM observation.

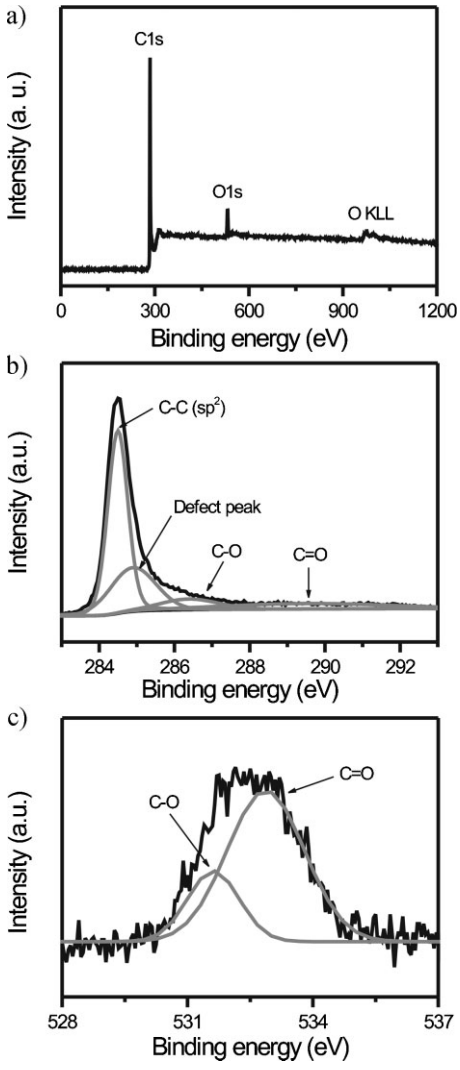

Figure 4. XPS spectra of MGNFs: survey scan (a); narrow scan for elements C 1s (b) and O 1s (c).

2.3. Chemical Composition of MGNFs

To study the effect of material composition on the growth and related properties, high resolution XPS technique was applied to investigate the chemical composition of MGNFs with different thicknesses at room temperature. Figure 4a is a typical XPS survey scan spectrum of MGNFs deposited with 40% methane, showing a strong C 1s peak at 284.5 eV, a small O 1s peak at 532.5 eV and a weak O KLL Auger band between 975–1014 eV. Except for some oxygen adsorbates on the surface because of the sample's exposure to air, no other elements were found in the film. The concentration of elements C and O in MGNFs was calculated to be about 94.9 and 5.1 at%, respectively. Figure 4b and c present a high resolution asymmetric C 1s and a weak O 1s XPS spectrum of MGNFs, respectively. After the subtraction of a Shirley background followed by fit using a mixture function of Lorentzian and Gaussian, the C 1s peak can be mainly deconvoluted into four sub-peaks at 284.5, 284.9, 286.4, and 289.5 eV, which have been assigned to C–C (sp^2), ''defect peak'', C–O and C=O bonds, respectively,[24] while the O 1s peak can be fitted by two Gaussian peaks at 531.7 and 532.9 eV corresponding to C–O and C=O bonds. Note, the ''defect peak'' with a 0.2–0.5 eV energy shift compared to C–C sp^2 hybridized bonds is sometimes mistakenly considered as the C–C (sp^3) bond, which usually is located at approximately 285.4 eV and can be found in the nanodiamond film and amorphous carbon etc.[25] This demonstrates that the MGNFs consist of metal-free graphitic materials with some oxygen adsorbates, as was confirmed by TEM and NEXAFS. The formation of such oxygen adsorbates is believed to result from the physical adsorption of oxygen or vapor mainly on the edge defects at room temperature, when the sample was exposed to air. The oxygen groups could exist in the form of C=O, O–C=O, COOH, and C–OH etc.[26] However, these surface functional groups formed by a room-temperature physical adsorption process differ from those created through the chemical oxidation and oxygen plasma treatment and are electrochemically inert owing to a weak interaction with the edge defect.

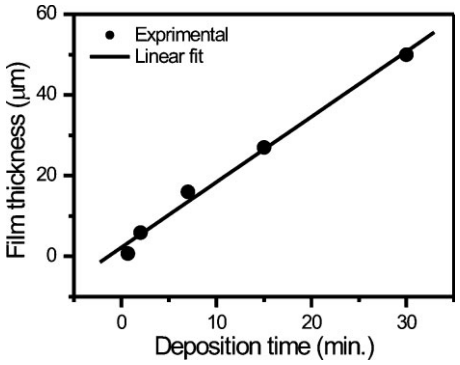

Figure 5. Thickness of MGNFs versus the deposition time.

2.4. Growth Rate of MGNFs

The large-scale synthesis of materials is prerequisite for their widespread application. The growth rate of MGNFs on Si was studied by changing the deposition time as shown in Figure 5. The MGNF samples were deposited for the duration between 40 s and 30 min under other identical conditions with 40% methane, which was found to have a faster growth rate. The thickness of MGNFs was carefully measured by SEM. An almost-linear relation between the thickness of MGNFs and the deposition time can be seen. The growth rate is calculated to be about 1.6 μm min^{-1}, which is 10 and 480 times larger than that of carbon nanowalls by bias enhanced MPCVD (10 μm h^{-1}) and radio-frequency plasma CVD (0.2 μm h^{-1}), respectively.[18,27] This demonstrates that our method is of high efficiency for growing MGNFs. Except for the slightly higher concentrations of methane used, the fast growth of MGNFs may be critically ascribed to the higher substrate temperature, which greatly increases the diffusion rate of hydrocarbon species on the Si surface. Moreover, another advantage in our method could lie in the use of nitrogen instead of hydrogen as the hydrogen plasma prefers to etch graphitic and amorphous carbon phases in the CVD process.

2.5. ET Dynamics of MGNFs

Since the highly graphitized sheets are metal free and possess a large amount graphitic edge planes on the surface, they present an ideal system for addressing the role of edge planes in electrochemical reactions. We firstly explored the electrochemical behavior associated with the ET reaction at the MGNF/solution interface using aqueous solutions containing $Fe(CN)_6^{3-/4-}$ redox couple.[28] This redox system was chosen because it has been well understood and used extensively with sp^2 carbon (e.g., graphite, glassy carbon, and CNTs etc.) and doped sp^3 carbon (e.g., diamond) electrodes. The ET reactions involving $Fe(CN)_6^{3-/4-}$ proceed by an inner sphere ET pathway with the electrode kinetics being sensitive to surface chemistry and microstructure as well as the density of electronic states near the Fermi potential. Figure 6a shows cyclic voltammetric (*C–V*) responses of about

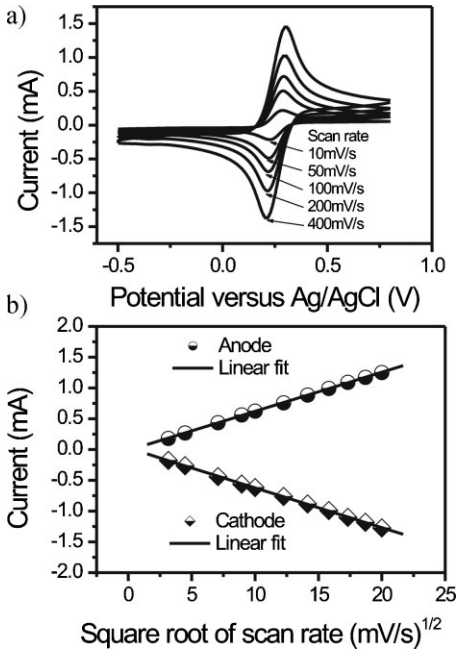

Figure 6. a) *C–V* profiles of the MGNF electrode in 5 mM ferrocouple with different scan rates from 10–400 mV s^{-1}; b) Anode and cathode peak currents versus the square root of scan rates.

8 μm thick MGNFs over the potential range of −0.5–0.75 V using different scan rates from 10 to 400 mV s^{-1}. It can be seen that the electrochemical response is a perfect reversible system with a peak-to-peak potential separation (ΔE_p) between 61.5–93.2 mV and a peak current ratio ($R_{a/c}$) of anode relative to cathode between 0.98–1.03. The peak-to-peak potential separation is related to the ET coefficient, and a low ΔE_p value (close to the ideal value of 59 mV) indicates a fast ET for a single-electron electrochemical reaction.[1] Here, the MGNFs were not subjected to any processing treatments after synthesis, including no special chemical functionalization activation procedures. The ΔE_p value obtained is very close to the ideal value of 59 mV at low scan rate, suggesting that a fast ET occurs between the MGNF surface and the electrolyte. One could argue that the low ΔE_p value could be attributed to the presence of oxygen functional groups observed by NEXAFS and XPS. These physically adsorbed oxygen groups was believed to possibly have an adverse effect on the ET rate, similar to that observed at the edge plane pyrolytic graphite (EPPG) electrode after prolonged exposure to air.[29] Figure 6b shows the oxidation and reduction peak currents as a function of the square root of scan rate between 10–400 mV s^{-1} for the 5th scan. The observed perfect linear relation reveals a single-electron Nerstian behavior where the electrochemical reaction is controlled by semi-infinite linear diffusion from the electrolyte to the electrode surface.

Theoretical studies have shown that the electronic structure of the electrode is important in determining heterogeneous electron kinetics between the electrode and the solution.[1] A high electronic density of states (DOS) in the electrode increases

ADVANCED FUNCTIONAL MATERIALS

the likelihood that an electron with the correct energy is available for electron transfer to a redox system. Compared to the basal planes of HOPG/graphene with a low DOS at the Fermi level, existing defects (such as kinks, steps, vacancies, etc.) on the edge planes/sites of HOPG/graphene can produce localized edge states between the conduction and valence bands, resulting in the high DOS near the Fermi level. Thus, the electrochemical reactivity at edge planes of HOPG is several orders of magnitude higher than those at basal planes of HOPG.[30] As we observed by SEM and TEM, MGNFs involve ensembles of a large number of vertical graphene nanoflakes with nanometer-scale sharp edges, where unambiguously there are more structural defects than those met in mechanically polished glassy carbon electrode (GCE) and EPPG. Rich edge defects lead to sufficient DOS being responsible for the fast electron transfer process observed.[31] However, the local edge state could be influenced by the defect type (e.g., armchair or zigzag) and surface adsorbates. This could explain why the ET rate is slightly slower than the ideal value, that is, such absorbed oxygen groups change the DOS near the Femi level. Meanwhile, the constituent graphene as a semimetal or a zero-gap semiconductor with remarkably high electron mobility at room temperature could enhance the electron transfer when its edge plane directly contacts the electrolyte.[6] Another important feature of the present platform has been the good electrical contact between the directly grown multilayer graphenes and the highly conductive Si substrate, which allows efficient electron transfer through the underneath Si. Thus, the superior ET kinetics of MGNF should be ascribed to the abundance of edge planes and defects, unique electronic structure of graphene and the good electrical contact with Si.

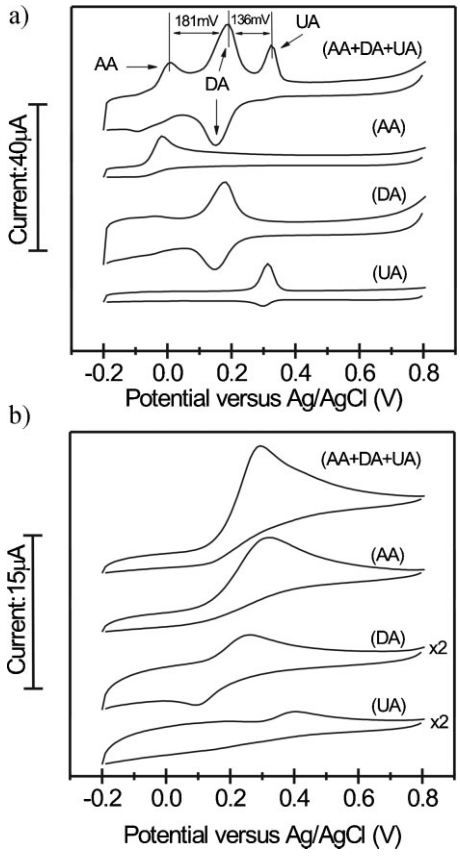

Figure 7. a) and b) *C–V* profiles of the MGNF and bare GCE electrodes, respectively, in the solution of 50 mM, pH 7.0 PBS with 1 mM AA, 0.1 mM DA, and 0.1 mM UA.

2.6. Selective Electrocatalysis and Biosensing Property of MGNFs

To demonstrate the selective electrocatalytic activity of the as-deposited MGNFs, we compared them with bare GCE toward the electrocatalytic oxidation of DA, AA, and UA, which all are essential biomolecules in our body fluids. Figure 7a and b illustrate the *C–V* curves obtained from 1.2 μm thick MGNF and bare GCE electrodes, respectively, in 50 mM 7.0 pH phosphate buffer solution (PBS) containing 1 mM AA, 0.1 mM DA and 0.1 mM UA and their ternary mixtures at a scan rate of 100 mV s^{-1}. It is clear that well defined and resolved voltammetric peaks are observed for the direct oxidation of AA, DA, and UA in the MGNF electrode in comparison to the GCE. For the oxidation of AA, similar irreversible *C–V* response with only an anodic peak located at −18.8 and 323.6 mV from the MGNF and GCE electrodes, respectively, can be observed. The negative shift of the anodic potential was estimated 342.4 mV. For the oxidation of DA, a redox pair was obtained with a ΔE_p of 30.2 mV and a $R_{a/c}$ of 1.43 at the MGNF electrode, whereas a ΔE_p of 161.1 mV and a $R_{a/c}$ of 1.20 were acquired at the GCE. The anodic potential at the MGNF electrode shifts 80.6 mV negatively compared with that of the GCE. For the oxidation of UA, a redox wave with a ΔE_p of 15.1 mV and a $R_{a/c}$ of 4.76 was observed at the MGNF electrode whereas no redox response was obtained at the GCE with the anodic peak located at 404.0 mV. The anodic potential at the MGNF electrode shifts 90.6 mV negatively compared with that of GCE. The negative shifts of the oxidation potentials together with the formation of well-defined redox peaks clearly indicate the faster ET kinetics and favorable electrocatalysis for the oxidation of all biomolecules at the MGNF electrode. For the ternary mixture of AA, DA, and UA, three strong anodic peaks are observed at 6.4, 187. 6, and 323.6 mV, respectively, at the MGNF electrode. A strong cathodic reduction peak of DA at 152.4 mV can also be observed. The GCE electrode presents a *C–V* response with only one anodic peak at 293.4 mV similar to the oxidation of AA. It is evident that the MGNF has a strongly electrocatalytic capability to simultaneously discriminate AA, DA, and UA.

Figure 8a shows differential pulse voltammetric (DPV) curves taken from the MGNF electrode in a 50 mM, pH 7.0 PBS solution containing 1 mM AA, 0.1 mM UA, and different concentrations of DA from 1 to 100 μM. Three peaks corresponding to the oxidation of AA, DA, and UA can be observed. At the concentration range of DA from 1 to 50 μM, the peak intensities of AA and UA remain unchanged while the peak of DA increases. At the concentration range of DA from 50 to 100 μM, the peak

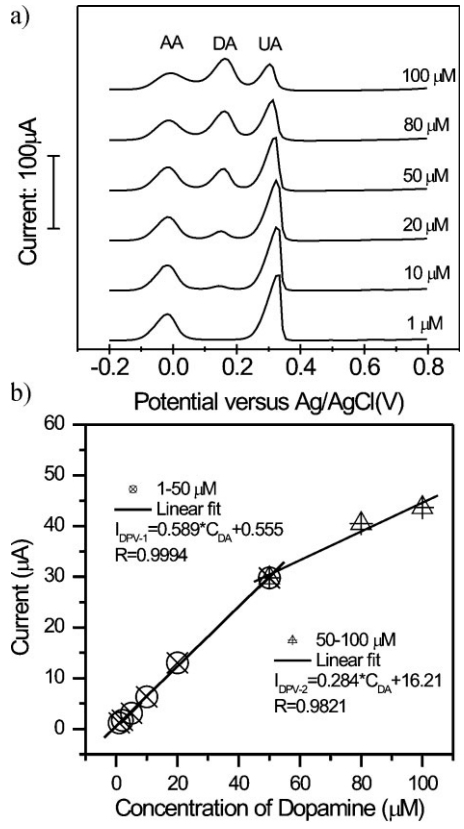

Figure 8. a) DPV profiles of the MGNF electrode in 50 mM, pH 7.0 PBS solution with 1 mM AA, 0.1 mM UA and different concentrations of DA from 1 to 100 μM; b) Peak current of DPV as a function of the concentration of DA. The linear regression equations and *R* were shown in the inset.

intensities of AA and UA slightly decrease and get broader while the peak of DA keeps increasing. Figure 8b illustrates the peak current of DPV as a function of the concentration of DA. It reveals that there are two different linear relations between the DPV peak current intensity (I_{DPV}) and the DA concentration (C_{DA}). The linear fit regression equations were

$$I_{DPV-1}(\mu A) = 0.589 * C_{DA} + 0.555 \quad (2)$$

and

$$I_{DPV-2}(\mu A) = 0.284 * C_{DA} + 16.21 \quad (3)$$

for the concentration range of DA from 1 to 50 μM and from 50 to 100 μM, respectively. In the low concentration range of DA, the peak intensity shows a perfect linear relation with the correlation coefficient (R) of 0.9994 while at the high concentration it shows a poor linear relation with $R = 0.9821$. Theoretical detection limit (DL, ratio of signal to noise = 3) was estimated about 0.17 μM based on 20 repeating measurements of DPV in the blank solution followed by a statistical calculation.

In terms of the DL and capability for determining DA, AA and UA simultaneously, the performance of MGNF electrode is superior to all other conventional solid state electrodes (e.g., GCE, boron doped diamond, and gold electrodes etc.)[32] and only comparable to that of EPPG electrode[33] (DL for DA is 0.09 μM with different interfering agents). Both MGNF and EPPG electrodes are free of metal catalysts and possess a plethora of edge planes, where there are a large amount of edge defects such as the kinks, steps, vacancies, dangling bonds, and so on. These edge defects could have different electrochemical interaction potential with the biomolecules of interest. They could be also locally negatively charged due to structural motifs, unpaired electrons or surface polarizations,[34] then repel UA and AA anions and form a molecular sieve permeable only to cationic DA.[13] As far as the possible effect of the surface oxygen functional groups on the simultaneous determination of such biomolecules is concerned very recently, it was found that the ratio of O to C (O/C) is very important in the determination of DA, UA and AA. It was shown that the electrochemically oxidized carbon electrodes with the O/C ratio up to 7 at% have no ability to distinguish the three biomolecules.[35] Here, not only the O/C ratio (5 at%) on the MGNFs is less than 7 at% but also the oxygen functional groups are inactive, as they formed by a room-temperature physical adsorption rather than by an electrochemical oxidation or oxygen plasma treatment. This evidences that the oxygen functional groups on MGNFs played a negligible role in the simultaneous detection of the three biomolecules. Thus, the edge planes/defects of MGNFs mainly facilitate enhanced electrochemical reactions with the biomolecules resulting in sensitive, well defined and resolved responses. The absence of any metal impurities unambiguously excludes the possible contribution of metal catalysts to the electrochemical performance. Generally, the separation of the oxidation peaks of DA, AA, and UA from each other has been a challenge using bare electrodes. For this purpose various modified electrodes have been constructed (e.g., titanate nanotube, ionic liquid, oracet blue, nafion/CNT coated poly(3-methylthiophene) modified electrodes etc.).[13,17] Although in some reports the DL is in the nM level, the used electrodes often need a complicated modification. The present MGNF electrode is fabricated simply and efficiently by a one-step CVD process without time-consuming elaborate modifications and/or functionalization procedures, which are commonly required in the majority of various modified electrodes.

2.7. Stability of MGNFs

The stability of the MGNF electrode regarding the electrooxidation of biomolecules was checked by prolonging the number of scans up to 300 as shown in Figure 9a and b. Note the sample with a thickness of about 8 μm was immerged in the electrolyte for at least 30 min to produce a stable surface and avoid variations induced owing to the initial hydrophobicity or capillary effects of MGNFs. Between the 1st–5th scan, an anodic peak current loss up to 17% can be observed at the C–V profiles, most likely arising from the unstable surface adsorbates involved in the electrochemical process.

ADVANCED FUNCTIONAL MATERIALS

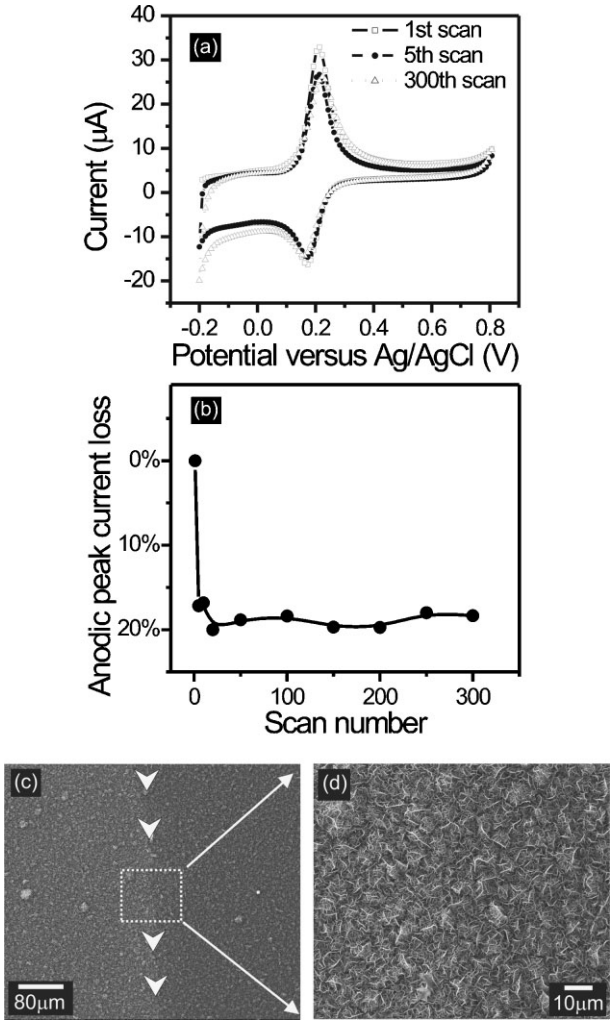

Figure 9. a) *C–V* profiles of the MGNF electrode in 50 mM, pH 7.0 PBS with 0.1 mM DA; b) Anodic peak current loss as a function of scan numbers for the electro-oxidation of DA; c) SEM image of MGNF electrode before and after long-term cycling with a clear boundary line; d) Enlarged SEM image of (c), showing no obvious changes in the MGNF morphology.

After the 5 scans, the diffusion between the electrode surface and the bulk electrolyte has reached a balance, and the standard deviation of peak currents up to 300 scans, is quite small in the range of 1–2%. To get a further insight into the high electrochemical stability of MGNFs, we used SEM to check the morphological changes on MGNFs after immersion in the electrolytes. Figure 9c and d show different magnification SEM images of thick MGNFs before and after long-term cycling. The morphology of MGNFs remains unchanged after long-term cycling. Unlike long CNTs, thick MGNFs do not accumulate together to form pyramid-like or 3D scaffold structures,[36] which result in a severe transformation of the surface areas. This evidences that MGNFs are mechanically robust structures, and have a strong adhesion with the Si substrate. They lead to the super electrochemical stability of MGNFs much better than that of CNTs or other carbon material modified GCEs, whose integrated structures by drop casting or dip coating are not stable and can be easily altered by the long-term electrolyte washing. So, the MGNFs provide one of the simple, reliable, and efficient electroanalytical platforms for the determination of biomolecules.

3. Conclusions

We have successfully demonstrated a simple method without use of catalysts to efficiently grow MGNFs on Si substrates with the growth rate as high as 1.6 μm min^{-1}. The MGNFs are made of highly graphitized knife-edge nanoflakes with a 2–3 nm thick sharp edge and have a preferentially vertical orientation relative to the Si substrate. The ET, electrocatalytic and biosensing properties of MGNFs were systematically investigated for the first time by employing the $Fe(CN)_6^{3-/4-}$ redox probe, electro-oxidizing biomolecules (DA, AA, UA) and sensing DA in the presence of high concentration of AA and UA, respectively. The MGNFs clearly demonstrated not only ideal ET kinetics but also well resolved simultaneous discrimination of AA, DA, and UA as well as the sensing ability of DA with the detection limit of 0.17 μm. The biosensing performance is superior to all other untreated, unmodified carbon based electrodes and is comparable only to the EPPG electrode. The remarkable ET kinetics, active electrocatalysis and sensitive sensing properties of MGNFs are mainly due to edge plane sites/defects that occur at the end of the vertical graphene nanoflakes, and their ability to act essentially as nanoconnectors that electrically transport the electrons to the underneath substrate. It should be emphasized that the presence of active edge sites makes MGNFs readily amenable to functionalization. The combination of edge plane reactivity together with the special nest-like morphology and large surface area of MGNFs present a distinct opportunity for creating a new class of electrodes for a wide range of applications in the electroanalytical, biosensing, energy storage/conversion sectors similar to those encountered by CNTs.

4. Experimental

The growth of MGNFs was carried out in a 1.5 KW, 2.45 GHz MPCVD system (Seki Technotron). Briefly, a 10×10 mm^2 heavily doped Si wafer (electrical resistance <0.004 *Ohms*) was cleaned with acetone and then positioned on the top of a thicker Si supporter located in the center of a circular Mo holder. This kind of the substrate-lift-up configuration not only allowed the substrate to be directly irradiated by plasma to higher temperature, but also prevented the substrate from being contaminated by the metal holder. After pumping the chamber down less than 10^{-2} Torr, the substrate was firstly pre-treated in the nitrogen plasma of 900 W at a pressure of 40 Torr for several minutes. Then, the growth of MGNFs started, by introducing methane into the chamber with various ratios relative to nitrogen and raising the microwave power to 900–1300 W. The substrate was heated by both high frequency induction coil and plasma up to more than 1000 °C, which was monitored by an infrared optical pyrometer from a top window of the chamber.

C–V and DPV measurements were carried out at a three-electrode Autolab electrochemical workstation at room temperature. A saturated Ag/AgCl solution, a platinum wire and as-deposited MGNFs on the Si substrate were used as the reference, counter and working electrodes, respectively. The cell would be either a small volume glass beaker or a self-made plastic cylinder vessel. In the beaker, electrical connections were made through the front MGNF surface of the electrodes. The back side of the Si substrate was covered by an insulting tape, to allow electrochemical reaction only with the MGNF surface. In the vessel, the thin film based planar working electrode can be well sealed at the bottom with a 5 mm diameter O ring and only a certain projected working area of 0.196 cm^2 was allowed to be exposed to the electrolyte. A 3 mm diameter GCE was polished with 0.25 μm Al_2O_3 slurry and then ultrasonically cleaned with ethanol and de-ionized water for comparison purposes. All experiments were performed by cycling at least 5 scans until the electrochemical reaction became stable. The redox system used for the evaluation of ET kinetics was $Fe_4(CN)_6$ (5 mM) and $Fe_3(CN)_6$ (5 mM) dissolved in KCl (1 M) buffer solution. For the electrocatalytic and biosensing study, the PBS (50 mM) was prepared by dissolving NaH_2PO_4 and Na_2HPO_4 in de-ionized water and adjusting the pH value to 7.0 with H_3PO_4 and NaOH. DA (0.1 mM), AA (1 mM) and UA (0.1 mM) with analytic reagent grade were freshly dissolved in the PBS for use in electrocatalytic and biosensing experiments in which all solutions were pre-deoxygenated by bubbling high-purity nitrogen for approximately 10 minutes.

Received: July 9, 2008
Published online: October 17, 2008

[1] R. L. McCreey, in *Electroanalytical Chemistry*, Vol. *17*(Eds: A.J. Bard), Marcel Dekker, New York **1991**, pp. 221–374.
[2] T. J. Davies, M. E. Hyde, R. G. Compton, *Angew. Chem. Int. Ed.* **2005**, *44*, 5121.
[3] C. E. Banks, A. Crossley, C. Salter, S. J. Wilkins, R. G. Compton, *Angew. Chem. Int. Ed.* **2006**, *45*, 2533.
[4] C. P. Jones, K. Jurkschat, A. Crossley, R. G. Compton, B. L. Riehl, C. E. Banks, *Langmuir* **2007**, *23*, 9501.
[5] M. Pumera, *Langmuir* **2007**, *23*, 6453.
[6] A. K. Geim, K. S. Novoselov, *Nat. Mater.* **2007**, *6*, 183.
[7] N. G. Shang, F. C. K. Au, X. M. Meng, C. S. Lee, I. Bello, S. T. Lee, *Chem. Phys. Lett.* **2002**, *358*, 187.
[8] a) Y. H. Wu, P. W. Qiao, T. C. Chong, Z. X. Shen, *Adv. Mater.* **2002**, *14*, 64. b) Y. Ando, X. Zhao, M. Ohkohchi, *Carbon* **1997**, *35*, 153.
[9] J. J. Wang, M. Y. Zhu, R. A. Outlaw, X. Zhao, D. M. Manos, B. C. Holloway, V. P. Mammana, *Appl. Phys. Lett.* **2004**, *85*, 1265.
[10] N. G. Shang, T. Stealer, X. Jiang, *Appl. Phys. Lett.* **2006**, *89*, 103112/1.
[11] R. M. Wightman, L. J. May, A. C. Michael, *Anal. Chem.* **1988**, *60*, 769A.
[12] a) J. M. Zen, C. T. Hsu, Y. L. Hsu, J. W. Sue, E. D. Conte, *Anal. Chem.* **2004**, *76*, 4251. b) R. Aguilar, M. M. Dávila, M. P. Elizalde, J. Mattusch, R. Wennrich, *Electrochim. Acta* **2004**, *49*, 851. c) Y. Li, X. Lin, *Sens. Actuators B* **2006**, *115*, 134. d) Y. Zhao, Y. Gao, D. Zhan, H. Liu, Q. Zhao, Y. Kou, Y. Shao, M. Li, Q. Zhuang, Z. Zhu, *Talanta* **2005**, *66*, 51. e) W. C. Poh, K. P. Loh, W. D. Zhang, S. Triparthy, J. S. Ye, F. S. Sheu, *Langmuir* **2004**, *20*, 5484.
[13] a) A. Safavi, N. Maleki, O. Moradlou, F. Tajabadi, *Anal. Biochem.* **2006**, *359*, 224. b) H. R. Zare, N. Rajabzadeh, N. Nasirrizadeh, M. Mazloum Ardakani, *J. Electroanal. Chem.* **2006**, *589*, 60. c) H. S. Wang, T. H. Li, W. L. Jia, H. Y. Xu, *Biosens. Bioelectron.* **2006**, *22*, 664.
[14] D. M. Zhou, H. X. Ju, H. Y. Chen, *J. Electroanal. Chem.* **1996**, *408*, 219.
[15] K. Pihel, Q. D. Walker, R. M. Wightman, *Anal. Chem.* **1996**, *68*, 2084.
[16] M. B. Gelbert, D. J. Curran, *Anal. Chem.* **1986**, *58*, 1028.
[17] a) A. H. Liu, M. D. Wei, I. Honma, H. S. Zhou, *Adv. Funct. Mater.* **2006**, *16*, 371. b) P. Wang, Y. X. Li, X. Huang, L. Wang, *Talanta* **2007**, *73*, 431.
[18] K. Tanaka, M. Yoshimura, A. Okamoto, K. Ueda, *Jpn. J. Appl. Phys. Part 1* **2005**, *44*, 2074.
[19] A. T. H. Chuang, J. Roberson, B. O. Boskovic, K. K. K. Koziol, *Appl. Phys. Lett.* **2007**, *90*, 123107/1.
[20] N. G. Shang, C. P. Li, W. K. Wong, C. S. Lee, I. Bello, S. T. Lee, *Appl. Phys. Lett.* **2002**, *81*, 5024.
[21] S. Banerjee, T. Hemraj-Benny, S. Sambasivan, D. A. Fischer, J. A. Misewich, S. S. Wong, *J. Phys. Chem. B* **2005**, *109*, 8489.
[22] G. Abbas, P. Papakonstantinou, G. R. S. Iyer, I. W. Kirkman, C. L. Chen, *Phys. Rev. B* **2007**, *75*, 195429.
[23] M. Abbas, Z. Y. Wu, J. Zhong, K. Ibrahim, A. Fiori, S. Orlanducci, V. Sessa, M. L. Terranova, I. Davoli, *Appl. Phys. Lett.* **2005**, *87*, 51923.
[24] H. Estrade-Szwarckopf, *Carbon* **2004**, *42*, 1713.
[25] K. L. Ma, J. X. Tang, Y. S. Zou, Q. Ye, W. J. Zhang, S. T. Lee, *Appl. Phys. Lett.* **2007**, *90*, 92105.
[26] K. Ihm, T. H. Kang, D. H. Lee, S. Y. Park, K. J. Kim, B. Kim, J. H. Yang, C. Y. Park, *Surf. Sci.* **2006**, *600*, 3729.
[27] M. Hiramatsu, K. Shiji, H. Amano, M. Hori, *Appl. Phys. Lett.* **2004**, *84*, 4708.
[28] J. Li, A. Cassell, L. Delzeit, J. Han, M. Meayyappan, *J. Phys. Chem. B* **2002**, *106*, 9299.
[29] X. B. Ji, C. E. Banks, A. Crossley, R. G. Compton, *ChemPhysChem.* **2006**, *7*, 1337.
[30] a) K. R. Kneten, R. L. McCreery, *Anal. Chem.* **1992**, *64*, 2518. b) R. L. McCreery, *Chem. Rev.* **2008**, *108*, 2646.
[31] a) K. Kobayashi, *Phys. Rev. B* **1993**, *48*, 1757. b) Y. Kobayshi, K. Fukui, T. Enoki, K. Kusakabe, Y. Kaburagi, *Phys. Rev. B* **2005**, *71*, 193406.
[32] a) J. Weng, J. Xue, J. Wang, J. Ye, H. Cui, F. Sheu, Q. Zhang, *Adv. Funct. Mater.* **2005**, *15*, 639. b) X. Huang, H. Im, O. Yarimaga, J. Kim, D. Lee, H. Kim, Y. Choi, *J. Phys. Chem. B* **2006**, *110*, 21850.
[33] R. T. Kachoosangi, R. G. Compton, *Anal. Bioanal. Chem.* **2007**, *378*, 2793.
[34] J. M. Carlsson, M. Scheffler, *Phys. Rev. Lett.* **2006**, *96*, 46806.
[35] K. S. Prasad, G. Muthuraman, J. M. Zen, *Electrochem. Commun.* **2008**, *10*, 559.
[36] M. A. Correa-Duarte, N. Wagner, J. Rojas-Chapana, C. Morsczeck, M. Tie, M. Giersig, *Nano Lett.* **2004**, *4*, 2233.